Research Square

Preprints are preliminary reports that have not undergone peer review.
They should not be considered conclusive, used to inform clinical practice,
or referenced by the media as validated information.

Mapping glioblastoma spreading: connexin43 and glial dynamic in the mouse and human microenvironment

Assunta Virtuoso

assunta.virtuoso@unicampania.it

University of Campania "Luigi Vanvitelli"

Giampaolo Milior

Collège de France, CNRS, INSERM, Labex Memolife, Université PSL

Ciro De Luca

University of Campania "Luigi Vanvitelli"

Julien Moulard

Collège de France, CNRS, INSERM, Labex Memolife, Université PSL

Luca Riccio

University of Campania "Luigi Vanvitelli"

Alesya Evstratova

Collège de France, CNRS, INSERM, Labex Memolife, Université PSL

Anaïs Venard

Collège de France, CNRS, INSERM, Labex Memolife, Université PSL

Giovanni Cirillo

University of Campania "Luigi Vanvitelli"

Johann Pallud

UMR S1266, INSERM, IMA-BRAIN, Université de Paris

Gilles Huberfeld

Collège de France, CNRS, INSERM, Labex Memolife, Université PSL

Nathalie Rouach

Collège de France, CNRS, INSERM, Labex Memolife, Université PSL

Michele Papa

University of Campania "Luigi Vanvitelli"

Research Article

Keywords: Astrocytes, Microglia, extracellular matrix, GFAP, GAP19, hemichannels

Posted Date: October 14th, 2026

DOI: https://doi.org/10.21203/rs.3.rs-11095851/v1

License: This work is licensed under a Creative Commons Attribution 4.0 International License.
Read Full License

Additional Declarations: No competing interests reported.

Abstract

High-grade gliomas (HGGs), including astrocytoma and glioblastoma (GBM), constitute the most prevalent primary tumors of the central nervous system (CNS). GBM cells demonstrate a notable ability to infiltrate the brain parenchyma, precluding complete surgical resection. Here we investigated the spreading of GBM cells and the response of the CNS microenvironment focusing on glial cells, which are essential interactors to GBM.

We used acute and organotypic slices from the mouse brain and peritumoral cortex of patients with HGGs. We found that human peritumoral tissue from cortical resection was characterized by high levels of the astrocytic Connexin43 protein (Cx43) and discrete infiltration of microglia. In contrast, the tumor core exhibited high myeloid infiltration and an altered extracellular matrix (ECM) composition, which was poor in CD44. We tracked mouse and primary human-labeled-GBM cells in 2D cultures and in co-culture with organotypic slices generated from mouse brain and human peritumoral tissues.

We found that the implanted GBM cells infiltrated the brain tissue, implying early glial modifications including an increase in Cx43 expression and distribution. Furthermore, the blockage of Cx43 hemichannels was accompanied by morphological changes and polarization of human GBM cells, typical for migration phenomena. The present study sheds light on the dynamics of GBM cells spreading in the living brain tissue, suggesting that the progression of the tumor correlates with changes within the host brain. Our findings identify the upregulation of Cx43 expression as a highly consistent modification in both mouse and human tissue that may be crucial for GBM infiltration.

1 Introduction

Diffusely infiltrating gliomas, including glioblastomas, astrocytomas, and oligodendrogliomas, are the most common type of primary brain tumors. Glioblastoma (GBM) cells have a remarkable capacity to diffusely invade the brain, making complete surgical resection impossible. Thus, the dispersion of GBM cells is a major obstacle for treating these tumors [1]. The patterns of GBM invasion are not random [2]. Rather, glioma cells tend to migrate with certain preferred paths such as along blood vessels or fiber tracts [3]. The majority of the GBM migrate along the corpus callosum and anterior commissure to reach the contralateral hemisphere [4, 5]. To accomplish this, tumor cells squeeze through tight spaces of the brain parenchyma, modifying the microenvironment structure and functional networks.

All multicellular systems function through dynamic and coordinated action of cell circuits, changing their activity in response to environmental signals, with time stamps into cells and a plethora of time-dependent transcriptomic, signaling and cell-cell interaction [6]. Differentiated GBM cells, adherent or migratory, keep contact within the extracellular matrix (ECM) [7], integrate into the neuroglial circuits and modify their functional aspects [8, 9]. Among the early interactions, the GBM deals with the brain innate immune system represented by astrocytes and microglia [10]. In vivo imaging showed that microglial cells sense the glioblastoma and become activated as soon as 30 min after the tumoral cells seeding [11]. Unlike the microglia, astrocytes are uniquely enriched in the peritumoral area [12] and form a sheet-

like structure at the tumor edge, being physically connected with the tumor, in particular via the gap-junction protein Connexin43 (Cx43) [13, 14]. As a consequence, electrical activity is altered and cortical plasticity is triggered [15, 16]. Notably, GBM cells exhibit autonomous Ca^{++} oscillations that affect the network activity, altering the physiological brain rhythm and contribute to treatment resistance[17, 18].

Astrocytes play a pivotal role in the GBM development, progression and therapeutic outcomes. Multiple signaling pathways have been described [19]. However, the role of glial Cx43 is still under debate. Cx43 is a multifunctional protein, with channel, hemichannel and non-channel functions. Cx43 is a ubiquitous protein, predominantly expressed by astrocytes, and it is involved in the formation of electrical synapses among the functions [20]. The channels are involved in cell-cell communication and are essential for brain homeostasis and calcium signaling [21]. The hemichannels (HCs) are instead involved in autocrine and paracrine communication. GBM appears to release ATP, glutamate and extracellular vesicles (EVs) via the hemichannels for signaling to astrocytes, microglia, and other CNS cells [22–24]. Therefore, glial Cx HCs play a major role in purinergic signalling and ECM remodeling, tissue hyperexcitability and epileptogenesis [25–27]. The pharmacological inhibition of Cx HCs has been shown to alleviate neuroinflammation, blood-brain barrier dysfunction, and suppress seizure activity in animal models [28, 29]. Furthermore, a monoclonal antibody that inhibits Cx26, Cx30 and Cx32 HCs has been demonstrated to be efficacious in both disrupting GBM progression and reducing hyperexcitability in mouse and human preclinical models [30]. The inhibition of Cx43 channel C-terminus has been implicated in sensitization to the chemotherapeutic agent temozolomide [31].

A role for Cx43 has been suggested in brain tumor invasiveness [32], as in a syngeneic intracranial mouse glioma model, Cx43-mediated intercellular communication between astrocytes is involved in the spreading of glioma cells into the brain parenchyma [33]. Yet whether Cx43 expression and distribution are regulated by GBM infiltration in the remodeled resident tissue is unknown. To investigate this possibility, we characterized the progression of mouse and eGFP-labeled human glioblastoma cells into mouse and human organotypic brain slices, respectively. The present study sheds light on the dynamics of GBM cell infiltration in living brain tissue and suggests that GBM progression induces structural modifications in the peritumoral microenvironment, with involvement of the Cx43. Blockade of Cx43 hemichannels induces morphological changes and polarization of human GBM cells. Altogether, these effects are similar in mouse and human tissues, suggesting conserved mechanisms across species and translational value of the present research.

2 MATERIALS AND METHODS

2.1 Murine Glioblastoma cell culture

The murine glioma GL261 cells were purchased from Creative Bioarray (cod. CSC-C9184W). GL261 cell line is a well-characterized and widely used model to investigate GBM cell biology, heterogeneity and immunotherapy [34]. GL261 cells were cultured in 90% Dulbecco´s MEM + 10% h.i. FBS as suggested by the manufacturer, or in B12-enriched medium (Neurobasal-A, 2% B12 supplement, 1% N2 supplement, 1%

glutamine, 0.5% glucose, 10 U/mL penicillin, and 100 µg/mL streptomycin) for the co-cultures with mouse organotypic slices [35].

2.2 Generation of eGFP Expressing Human Tumor Cells

Human primary tumor cells characterized as GBM cells were gently provided by GlioTex facility (Prof. A Idbaih and Dr. M Verreault). Human primary GBM cells were genetically modified to express eGFP using lentiviral vector. GBM cells were called as N2 and were transfected with the pEGFP-N1 expression vectors (Clontech), grown in selection medium containing G418 (500 lg/ml), and then FACS-sorted to select cells expressing high levels of eGFP. This method yielded populations of glioma cells in which greater than 95% of the cells expressed the green fluorescent protein (GFP). N2 cells were grown in DMEM/F12 (Life Technologies,31331028), 100 UmL − 1/0.1 mgmL − 1 Pen-Strep, B27 supplement 50x (Life Technologies, 17504-044), Human FGF Basic (Peprotech, 100-18B), Human EGF (Peprotech, 100 − 15).

2.3 Animals

Young adult (3–5 week-old) C57Bl/6 mice (Envigo) (*n* = 30) were included in the present study. Animal care was in compliance with the Italian and European Guidelines for use and care of laboratory animals (EU Directive 2010/63) under the authorization no. 268/2012-B from the Minister of Health. Each animal was given free access to food and water, under a 12/12 h light/dark cycle.

2.4 Patients

The present study includes human brain tissues from 13 patients affected by glioma. Most cases were astrocytoma IDH1-mutant (R-132-H) (10/13; 77%), followed by oligodendroglioma IDH-mutant-1p/19q-codeleted (3/13; 23%). Most patients (11/13; 84.6%) had epileptic seizures at diagnosis. The samples were collected at Sainte-Anne Hospital and La Pitié-Salpêtrière Hospital (Paris, France). This study was approved by the Comité d'Evaluation et d'Ethique de l'INSERM - IRB00003888 (approval n°21–864). Subjects' consent was obtained according to the Declaration of Helsinki.

2.5 Preparation of brain acute and organotypic slice cultures from young adult mouse

- Animals were rendered unconscious using isoflurane gas, and then euthanized by cervical dislocation. Brains were dissected and coronal slices (300 µm) were cut using a vibratome (Campden Instruments, 5100mz), while maintaining the sterility, as previously reported [36]. Mouse slices to culture were transferred in 70 µm cell strainer with fresh, RT carbogen-oxygenated ACSF (artificial cerebrospinal fluid) for recovery (45 min). Slices were cultivated in B12-enriched medium, as per the GL261 cell culture. Brain tissue cultures were maintained in a humidified atmosphere with 5% CO2 at 35°C. The medium was replaced three times a week. The young adult mouse organotypic slices were cultured up to 7 days in vitro (div).

2.6 Preparation of human acute and organotypic slice cultures

Surgical specimens were obtained from patients with glioma. During surgery, a small block of cortical tissue was removed as a safety margin with respect to the glioma supratotal surgery approach. It was immediately placed in ice-cold sucrose ACSF along with a piece of tumor core, and transferred to the laboratory. The tissue was processed as previously described [37]. Briefly, the tissue piece was immerged in carbogen-oxygenated ACSF, cleaned of blood clots, vessels and meninges, and cut in 350 µm thick slices using the vibratome (Leica VT1200) at low speed (0.1 mm/sec). Each acute slice to be processed was immediately transferred to the interface chamber for recordings, while others were fixed in Zinc Formalin Fixative (ZFF) (Sigma-Aldrich, Z2902).

Human slices to culture were transferred in cell strainers with fresh, RT carbogen-oxygenated ACSF for recovery (45'min). After that, they were cultured for 1 h in NCS medium, in incubator with 5% CO2 at 37°C. The NCS is composed of 50% Neurobasal-A, 50% DMEM, Hepes 20mM, 2% B27 supplement, 1% N2 supplement, 1% Glutamax, 100 UmL – 1/0.1 mg mL-1 Pen Strep, and 1% NEAA. The NCS medium was replaced with fresh human cerebrospinal fluid (hCSF), which was changed three times per week. The human organotypic slices were cultured up to 7 DIV.

2.7 Viability test for GBM cells and organotypic slices cultures

Cell viability was assessed using 3-[4,5-dimethylthiazol-2-yl]-2,5 diphenyltetrazolium bromide salt (MTT) (Sigma-Aldrich), as previously described [38]. Briefly, GL261 cells were seeded at a density of 1×10^4 cells/well in 100 µL of B12-culture medium, in 96-well plates. At confluence, the medium was replaced with fresh medium with MTT salt added to each well for 4 h at 37°C. 100 µL of Dimethyl sulfoxide (DMSO) were used to dissolve formazan salts for 15 min at 37°C, and absorbance was measured at 570 nm in a plate reader (Parkinelmer, Victor Nivo). Three replicate wells were used for each group. DMSO was used as a blank; GL261 cells treated with 10 mM H_2O_2 were used as the negative control.

Organotypic brain slice cultures were incubated in sterile dPBS with MTT substrate for 20 minutes at 37°C. Additional fresh brain slices in dPBS containing 4% paraformaldehyde (PFA) were included in the analysis as the negative control. Afterwards, brain slices were transferred into fresh tubes and DMSO was added in a volume proportional to the slice weight to dissolve the violet formazan crystals formed during the assay. The samples were then centrifuged and 100 µL of the supernatant was transferred to a 96-well plate in duplicate. Absorbance was measured at 570 nm.

2.8 GBM cells injection in human and mouse organotypic slice cultures

The number of living and dead cells in culture was determined by cell counting after trypan blue staining as previously described [39]. Briefly, cells were dissociated with trypsin digestion. Cells suspension was

diluted 1:1 in trypan blue solution (Sigma Aldrich), incubated for 2 min and counted using a Burker chamber. Cell viability was determined based on the total cell count, the dilution factor and the trypan blue dye exclusion assay. For human and mouse cell transplants, N2 and GL261 cells were centrifuged and resuspended in PBS (10000 cells in 1 µL of PBS). They were immediately injected into the human cortical slices or cortex from whole brain mouse slices respectively, using a sterile patch-clamp tip connected to a syringe. GBM cells engrafted the slices and their integration could be observed in the following days as previously described [40].

2.9 Drug treatments

The synthetic peptide TAT-GAP 19 (> 85% pure) was obtained from GenScript (Piscataway, NJ, USA). YGRKKRRQRRR was the TAT sequence, which is responsible for the peptide's cell penetration [41]. Gap19 is a selective inhibitor of the Cx43 hemichannels (HC). It perturbs the carboxy-terminal interaction with a cytoplasmic loop (CL)-located binding site, leading to the Cx43 HC closure [42].

GAP-19 was dissolved in sterile ddH20 as per manufacturer’s instructions, at a final concentration of 200 µM, and added to the culture medium. Scramble peptide was administered in an identical manner. The half-life of Tat-Gap19 peptide was calculated with the peptide lifetime predictor (PlifePred, http://crdd.osdd.net/raghava/plifepred/) as described in [43].

GAP-19 peptide was provided to GBM cells or to human organotypic slices with or without GBM cells injection. The potential effects of GAP-19 on treated, untreated GBM cells, and human organotypic slices were investigated using dynamic microscopy. GBM cells and slices were fixed at 4 h from the last treatment and prepared for immunostaining.

2.10 Scratch (wound-healing) assay

To evaluate the effects of GAP19 on scratch closure, GL261 cells were seeded in 12-well plates and cultured until they reached approximately 90% confluence. A scratch was gently introduced into the cell monolayer using a sterile pipette tip. Cells were washed twice with culture medium to remove debris and incubated with GAP19 (200 µM) until the experimental endpoints (4 h and 24 h). Images were acquired using an IXplore IX73 Standard microscope (Evident). The distance between the two edges of the scratch was labeled and measured to assess wound closure. Scratch closure was quantified by counting the cells found within a predefined region of interest (ROI) inside the scratch, in at least four randomly selected fields per well. To ensure consistent analysis, the ROI was rotated to align with the orientation of the scratch while maintaining a constant size.

2.11 Ex Vivo electrophysiology: Multi Electrode Array (MEA) Recordings

- Human acute and organotypic slices were transferred in an interface chamber containing a standard artificial cerebrospinal fluid (ACSF; 119mM NaCl, 2.5mM KCl, 2.5mM $CaCl_2$, 1.3mM $MgSO_4$, 1mM NaH_2PO_4, 26.2mM $NaHCO_3$, and 11mM glucose, saturated with 95% O_2 and 5% CO2, at a

temperature of 37°C) for at least 1h. For multi-electrode array (MEA) recordings, slices were transferred on planar MEA petri dishes (200 – 30 ITO electrodes, organized in a 12x12 matrix, with internal reference, 30µm diameter and 200µm inter-electrode distance; Multichannel Systems, Germany). They were kept in place by using a small platinum anchor. The slices on MEAs were continuously perfused at a rate of 2 mL/min with a magnesium-free ACSF. Pictures of slices on MEAs were used to identify the location of the electrodes through the different cortex regions and to select the electrodes of interest. Data were sampled at 10kHz and network spontaneous activity was recorded at room temperature by a MEA2100-60 system (bandwidth 1-3000Hz, gain 2x, Multichannel Systems, Germany) through the MC Rack 4.5.1 software (Multichannel Systems, Germany) [44]. To boost tissue excitability, slices were then perfused with an “epileptogenic” ACSF, in which Mg^{2+} is absent and K^{+} is raised to 6 mM. Once the perfusion with 0 Mg^{2+} 6 mM K^{+} ACSF had started, the activity of cortical slices was recorded.

2.12 Dynamic Microscopy of GBM cells and Brain Slice Cultures

Dynamic photography was performed by taking a picture of the cells and slices from a single focal plan every 3 hours over a time frame of 7 days under a fluorescent, inverted microscope (Thermo Fisher Scientific, EVOS Microscope). N2 morphometry was quantified using ImageJ software (Rasband, W.S., ImageJ, U. S. National Institutes of Health, Bethesda, Maryland, USA, http://imagej.nih.gov/ij/, 1997–2011).

Mouse and human acute/organotypic slices were fixed in 4% PFA or zinc formalin, respectively, at 3 and 7 days post-injection (dpi). The immunostaining protocol was adjusted from previous publications [25, 45–47]. Briefly, the slices were incubated for blocking in 1% Tryton, 10% Serum in Pbs/NaN_3 and then with primary antibodies for 4 overnights (see Table 1). After washing in PBS, 3 over night incubation with the appropriate secondary antibodies (Alexa Fluor) and Dapi (4',6-diamidino-2-phenylindole) nuclear staining was performed. Tissues were imaged using a laser scanning confocal system microscope (Zeiss LSM 900). Two and three-dimensional reconstructions of brain tumor slices were generated from fluorescent micrographs.

GBM cell cultures were stained with a similar protocol, reducing incubation times (1 overnight for the primary antibodies, 2h for the secondary antibodies), and imaged using an inverted fluorescence microscope (Thermo Fisher Scientific, EVOS Microscope or IXplore IX73 Standard microscope, Evident).

2.13 Western Blotting

Brain slices and GL261 cells protein extraction was performed by adding 100µL of RIPA buffer (140 mM NaCl, 10 mM Tris-HCl pH 8.0, 1 mM EDTA, 1% Triton X-100, 0.1% SDS, 0.1% sodium deoxycholate, 1 mM PMSF) supplemented with fresh protease and phosphatase inhibitors (1% each). Sample homogenates were centrifuged at 14,000 rpm for 10 minutes at 4°C to separate the supernatant and pellet. The pellets were resuspended in 50 µL of RIPA buffer. Protein concentrations of both supernatant and resuspended

pellet were determined using a Bradford assay in 96-well plates and measured with a VICTOR Nivo plate reader (Revvity Life Sciences).

Samples were prepared for SDS-PAGE by mixing with 4× Laemmli Sample Buffer (60 mM Tris-HCl pH 6.8, 10% glycerol, 2% SDS, 100 mM DTT, 0.1% bromophenol blue) to a final volume of 15µL containing 30 µg of total protein. Proteins were resolved by SDS-PAGE using a discontinuous polyacrylamide gel system. After electrophoresis, proteins were transferred onto a nitrocellulose membrane using electroblotting. Successful protein transfer was verified by staining the membrane with 0.1% Ponceau Red in 5% acetic acid.

Membranes were blocked in 5% BSA in TBST (10 mM Tris HCl pH 7.5, 150 mM NaCl, 0.1% Tween 20) and incubated overnight with primary antibodies targeting the proteins of interest (see Table 1). Membranes were washed three times in TBST and then incubated with species-specific HRP-conjugated secondary antibodies. Following secondary antibody incubation, washing steps were repeated.

Detection was performed using enhanced chemiluminescence (ECL), and signals were captured using a LI-COR Digit imaging system (6-minute exposure). Densitometric analysis of protein bands was conducted using ImageJ software.

2.14 Measurements and Statistics

Raw data from MEA recordings were analyzed using MC Rack (Multi-Channel System, Reutlingen, Germany). Detection of bursts was performed using the “Spike Sorter” algorithm, which sets a threshold of the noise (5-fold), and low-pass filter. This allowed to automatically detect each event [44]. Measurements of immunofluorescence (IF), and western blotting (WB) markers were performed using ImageJ software (Rasband, W.S., ImageJ, U. S. National Institutes of Health, Bethesda, Maryland, USA, http://imagej.nih.gov/ij/, 1997–2011) in a blinded manner.

In particular, for the quantification of Cx43-positive cells, confocal z-stack images acquired using a Zeiss 40× objective were reconstructed in three dimensions using ZEN software (Zeiss, Oberkochen, Germany). The reconstructed image stacks were subsequently analyzed using Fiji/ImageJ. For each image, a fixed-size region of interest (ROI: 200 x 200 µm) was analyzed. Individual nuclei were identified based on 4',6-diamidino-2-phenylindole (Dapi) staining and used for cell counting and fluorescence measurements. Cx43 immunofluorescence intensity was measured in the perinuclear region associated with each nucleus, and cells were classified as Cx43-positive when the fluorescence intensity exceeded a predefined threshold. The same intensity threshold was applied to all images acquired under identical imaging settings. Data were exported and analyzed using the Graph Pad Prism 8.4 program (SPSS-Erkrath). Data were checked for normal distribution and homogeneity of variance by the Kolmogorov–Smirnov’s and Levene’s mean tests, respectively. Normal distributions with equal variances were analyzed by Student’s t tests for comparing two groups, and one-way ANOVA for multiple comparisons followed by all pairwise Holm–Sidak post hoc test. Kruskal–Wallis test was used for non-parametric analysis followed by Tukey’s test for pairwise multiple comparisons. Level of significance was set at p =

0.05 (*p ≤ 0.05; **p ≤ 0.01; ***p ≤ 0.001). Statistical techniques were employed to derive correlation coefficients and mutual information metrics for each feature. Results are expressed as group mean ± SEM and represented in the charts.

3 RESULTS

3.1 Characterization of Glioblastoma cells

We characterized GL261 cells and tested their viability in B12-enriched medium to obtain optimal murine brain slice-tumor co-cultures. GL261 cells have been characterized in detail [34]. They appear with the shape of fibroblastoids, but have a genetic profile similar to the primary human GBM, making them a very aggressive tumor. Among the phenotypic markers, GL261 express vimentin, not GFAP [34] .

In the B12-enriched medium, GL261 showed a morphological shift. They reduced their spherical shape (form factor, p = 0.0004, two-tailed unpaired t-test with Welch's correction) and occupied a larger surface area (cell area fraction (%), p = 0.0002, two-tailed unpaired t-test with Welch's correction) compared to the cells grown in the DMEM medium (standard). They formed adherent neurospheres in both conditions by reaching confluence (**Fig. 1a-c**). In the B12-enriched medium GL261 were viable at higher rates compared to the standard medium (One-way Anova, Tukey's multiple comparison test, p < 0.0001) (**Fig. 1d**). The morphological shift of GL261 indicates that tumor cells change from a rounded shape to a more active, proliferating state when provided with ample nutrients compared to the basic medium suggested by the manufacturer. However, they retained vimentin expression and did not express GFAP (**Fig. S1**).

Human primary N2 cells were cultured in DMEM/F12 supplemented with B27 1x, EGF 20ng/ml and b-FGF 20ng/ml. N2 cells had a similar aspect compared to the murine GL261 cells. N2 cells formed neurospheres. However, they expressed GFAP and Cx43 (**Fig. 1e, Fig S2**).

3.2 The neuroglial network changes among tumor and peritumoral tissues.

Brain specimens were collected from patients affected by glioma. Surgical tissues were classified as either "tumoral" or "peritumoral" based on intraoperative MRI-guided neuro-navigation data. Tissues obtained from areas within MRI FLAIR hypersignal or appearing as macroscopically infiltrated according to the neurosurgeons were considered as tumoral. Tissues dissected from areas outside such abnormal MRI zones and appearing macroscopically normal were considered as peritumoral [48]. Despite their macroscopically healthy appearance, peritumoral tissues may be sparsely infiltrated by tumor cells and exhibit cellular, molecular, and functional alterations [49].

To study the modifications of the human tumor microenvironment, we performed immunostainings in combination with antibodies that selectively label astrocytic-like cells (anti-Cx43), myeloid cells (anti-

Iba1), and the extracellular matrix receptor (anti-CD44), which has been proposed as an invasion marker for GBM [50].

Cx43 has a dynamic expression. It can be found with a dispersed cytoplasmic, perinuclear, or membrane localization [51]. However, the autofluorescence of the lipofuscin granules may interfere with the perinuclear targeting of the marker. For accurate analysis, we considered the mean density value related to the area of interest, with spatial exclusion parameters. Peritumoral pieces showed a high density for Cx43 compared to the tumoral pieces ($p = 0.0366$, two-tailed unpaired t-test with Welch's correction) (**Fig. 2a-b**). Cx43 expression correlates with CD44 levels during the GBM invasion [23]. Accordingly, we found a spatial, positive molecular distribution among the markers. Peritumoral acute slices showed a high CD44 density compared to the tumoral samples ($p = 0.02$, two-tailed unpaired t-test) **(Fig. 2a-c).**

Immunostaining analysis for the microglial Iba1 marker revealed that Iba1 density was higher in tumor pieces compared to the peritumoral tissues ($p = 0.021$, Kolmogorov-Smirnov test) **(Fig. 2d)**. Myeloid cells from the tumor core showed an increase of the area and a reduction of the mean processes length, typical of the macrophagic shape (regarding mean cell area, F test to compare variances; $*p = 0.0250$), (regarding processes length, $p = 0.0058$, two tailed unpaired t-test) **(Fig. 2e)** [5].

This evidence proves that the glial microenvironment in human high-grade gliomas and their peritumoral tissues potentially have a distinguished morphological and molecular profile, which could be crucial for disease predictions, modeling, and interventions.

3.3 Functional neuroglial networks in organotypic cultures.

It is known that organotypic culturing modifies the neuroglial networks and the adult tissue is fragile [52]. Electrophysiological recordings were performed for two complementary reasons. First, they provide a functional assessment of tissue viability and preservation of network activity, representing one of the few direct readouts from the human slices cultures. Second, neuronal network activity is a relevant parameter in glioma biology, as increasing evidence indicates that tumor progression and invasion are closely linked to interactions with electrically active neuronal circuits [53, 54].

We verified the vitality of our model by recording the electrical activity of selected organotypic slices with or without GBM cell transplantation and compared these recordings with acute human cortical slices. As previously reported by Dossi et al. [37], spontaneous activity in acute human cortical slices progressively increased over time. Under epileptogenic ACSF conditions (6 mM K^+, 0 mM $Mg2^+$), acute cortical slices displayed a significant increase in discharge frequency ($p = 0.0225$, F test for variance), while no significant changes were recorded in peak amplitudes (**Fig. 3a-c**).

Human organotypic slices cultured for 7 DIV, with or without GBM transplantation, remained electrically active. Although event frequencies tended to be lower than in acute slices, this difference was not statistically significant, whereas peak amplitudes remained unchanged **(Fig. 3a, d-e)**. These findings are consistent with network reorganization rather than a loss of network function.

Given the limited number of human biological replicates, these findings provide exploratory evidence that our organotypic model preserves tissue viability and functional neuronal network activity despite culture-induced remodeling of the neuroglial circuitry.

3.4 Transplanted Glioblastoma Cells Infiltrate the Organotypic Brain Slices

To characterize the GBM progression and microenvironment, we injected mouse GL261 cells and human e-GFP + GBM cells into the organotypic cortical tissue at div 1 in murine and human slices, respectively.

Adult mouse cultures retained their vitality for one week when injected with PBS compared to the fresh acute tissue (Acute 0.2906 ± 0.016; Org PBS 0.2233 ± 0.019). The young adult mouse cultures represented a fertile platform for the GL261 progression, as the vitality of the system triplicated (0.5516 ± 0.038, $p \leq 0.0001$, one-way ANOVA followed by Tukey's test for multiple comparisons) (**Fig. 4a**). Accordingly, the proliferating cell marker Ki67 was restricted to densely packed cell clusters with large nuclei (**Fig. 4b**).

We examined the distribution of transplanted eGFP-labeled GBM cells at 0, 3, and 7 dpi. eGFP-labeled GBM cells were localized either in multicellular clusters or as individual cells. GBM cells had a predominantly unipolar morphology, with a rounded cell body in the first dpi. eGFP GBM cells appear to increase branching in the following days and completely cover the tissue, both in the cortical gray and subcortical white matter (swm) (**Fig. 4c**), suggesting a spreading infiltration [1].

3.5 Glioblastoma Spreading modifies the microenvironment

To study the modifications of the glial microenvironment following GBM infiltration, we investigated the expression of the markers Cx43, GFAP, and Iba1 in both mouse and human organotypic slices injected with PBS or tumor cells.

Immunostainings for GFAP showed an increase in the fluorescent intensity in response to the murine GBM development comparing to the slices injected with PBS, suggesting a reaction of the resident astrocytes in the peritumoral tissue by 3 dpi (One-way Anova followed by Tukey's test for multiple comparisons, ORG PBS vs ORG GBM, $^{*}p = 0.0468$; Acute vs Org PBS, $^{\#}p = 0.0001$; Acute vs Org GBM, $^{\#}p = 0.015$) (**Fig. 5a-b**). We found an increase in Cx43 protein expression in mouse organotypic slices injected with GBM compared to the PBS delivery at 3 dpi (One-way Anova followed by Tukey's test, ORG PBS vs ORG GBM, $^{*}p = 0.0098$; Acute vs ORG PBS, $^{\#}p = 0.0001$; Acute vs. ORG GBM $^{\#}p = 0.0002$). (**Fig. 5b-c**). The increase in Cx43 expression may reflect a shift between its cytoplasmic and membrane form. Western blot analysis on soluble and insoluble tissue fractions showed an increase in the ratio Cx43 Cytoplasm/Membrane in the co-culture of mouse GBM-brain slices compared to the acute system or to the GL261 2D cultures (One-way ANOVA followed by Kruskal-Wallis test, Org GBM vs Gl261, $p = 0.0049$; Org GBM vs Acute, $p = 0.1570$) **(Fig. 5d-e)**.

Immunostainings in the human GBM-brain co-cultures system revealed an increase in cell number ($p = 0.0437$, two tailed unpaired t-test) positive for the perinuclear expression of Cx43 at 3 dpi **(Fig. 6a-b)**. Accordingly, it has been shown that the invasive pattern of the mesenchymal mode of human GBM may mimic an astrocytic-like microenvironment [55]. Altogether, these results indicate that Cx43 is involved in the CNS response to the GBM progression.

The myeloid component was affected by organotypic culturing (**Fig. 6c-e**). We found a basal decrease in Iba1 expression in the human organotypic models compared to acute conditions (one-way Anova, Dunnet's multiple comparisons test, ACUTE vs ORG PBS, $*p = 0.0264$; ACUTE vs ORG N2, $*p = 0.0415$) (**Fig. 6c-d**). Iba1-expressing cells indeed modified their area and reduced the length of the processes in the organotypic cultures at 3 dpi (regarding area, Ordinary One way Anova followed by Tukey's multiple comparisons test, ACUTE vs ORG PBS, $*p = 0.0334$; ORG PBS vs ORG N2, $^{\#}p = 0.0323$), (regarding processes length, Ordinary One way Anova followed by Tukey's multiple comparisons test, ACUTE vs ORG PBS, $*p \leq 0.0001$; ACUTE vs ORG GBM, $*p \leq 0.0001$) (**Fig. 6e**).

Altogether, these results show there are potential modifications involving resident astrocytes and myeloid cells in both organotypic models. This may support the spreading of GBM. Among the molecular features, Cx43 appears to be fine-tuned in the host tissue of both experimental models.

3.6 Cx43 hemichannels may have a role in GBM progression.

To dissect how the multifunctional Cx43 protein may work in GBM spreading, we treated GBM cells with GAP19, a selective blocker for Cx43 hemichannels, either in culture or in co-culture with brain tissue.

The scratch assay revealed that, at 4 h, the GAP19-treated group exhibited a higher number of cells within the region of interest (ROI) of the scratch compared with the corresponding control (CTR) group ($**p = 0.004$, Ordinary One way Anova followed by Tukey's multiple comparisons test). No significant difference in the number of cells within the ROI was observed between GAP19-treated and CTR groups at 0 h and 24 h **(Fig. 7a-b)**. GL261 cells responded with an upregulation of Cx43 protein at 4 h, and this effect was lost after 24 h (CTR = 1.477 ± 0.145; GAP19 4h = 2.426 ± 0.714; GAP19 24h = 0.867 ± 0.115; $^{\#}p = 0.014$, one-way Anova, Tukey's multiple comparisons test) **(Fig. 7c-d)**.

Human eGFP-GBM cells were longitudinally aligned and polarized from DIV 4 to DIV 7 under chronic treatment with GAP19 in culture and co-culture with human tissue **(Fig. 8a-b)**. Using time-lapse microscopy, we found that the circularity index of the GFP+ cell bodies in co-culture with brain tissue was significantly lower under GAP19 treatment ($p = 0.0006$, $p = 0.1921$, ordinary one-way Anova, Tukey's multiple comparisons test) **(Fig. 8c-d)**.

Altogether, these data indicate that both mouse and human GBM cells used in the present study respond to blockade of Cx43 hemichannels in a time-dependent manner. In murine GBM cells, GAP19 treatment was associated with an increased number of cells within the scratch region at 4 h and a rapid

upregulation of Cx43 protein expression. In contrast, human primary GBM cells exhibited changes in cell morphology and polarization following chronic GAP19 treatment.

Table 1
Primary Antibodies used

Target	Brand	Dilution
anti-GFAP	AB5804, Millipore	IF: 1:400
anti-Iba1	019-19751, WAKO	IF: 1:500
anti-Connexin43	A1978, C6219, Sigma-Aldrich	IF: 1:200; WB:1:1000
anti-Ki67	ab16667, Abcam	IF: 1:50
anti-CD44	Ab189524, Abcam	IF:1:200
Anti-β-actin	A5441, Sigma-Aldrich	WB: 1:10000

4 Discussion

GBM is a major challenge for research among brain diseases. The high intra- and intertumoral heterogeneity is one of the main barriers, impairing the translational value of rodent experimental models. However, organotypic slice culture enables the study of human tissue at 3D cellular and small network level, overcoming the temporal limits of the fresh tissue [56]. In this work, we characterized the glial components of human tumor and peritumoral tissue under both acute ex vivo and organotypic conditions, followed by the injection of primary GBM cells. We set up a parallel model of the mouse GBM brain to assess its translational potential. Tissues obtained from patients are always limited in extent. Having a parallel GBM mouse model offering the whole brain could thus be useful to predict the anatomical behavior of the tumor.

Despite structural and functional modifications of the neuroglial networks, the human and mouse organotypic slice cultures retained vitality for one week, shedding light on GBM biology and its microenvironment, and offering hints to fight this incurable disease. The electrophysiological recording of human slice cultures demonstrated they were biologically active after long-term maintenance. Importantly, electrophysiological activity represents a clinically relevant feature of glioma progression. Tumor-associated epileptic seizures are a hallmark of diffuse gliomas and have been associated with patient prognosis, with several studies reporting longer survival in glioma patients presenting seizures at diagnosis compared with non-epileptic patients [57]. Therefore, preserving measurable network activity in organotypic slices is not only an indicator of tissue viability but also an essential prerequisite for modeling physiologically relevant glioma–brain interactions.

The characterization of the fresh human tumor and peritumoral HGG revealed that the tumor core was entangled with myeloid cells. An abundance of macrophages at the tumor core is a hallmark of poor prognosis. Infiltrating macrophages are recruited at the tumor core in the advanced phase of the

disease, indicative of cancer recurrence at a short distance [5, 58]. Predicting the anatomical and biological behavior of GBM in the brain peritumoral area would be pivotal for planning clinical follow-up, selecting second-line treatments, and improving the quality of life for patients. Myeloid cells in the peritumoral zone of astrocytoma showed a diverse morphology, with a smaller area and longer processes compared to the tumor core, similarly to microglia cells. Rather, the peritumoral microenvironment was characterized by profound changes. Cx43 protein level was upregulated, as well as the CD44 protein. Astrocytic Cx43 in the peritumoral microenvironment affects microglial functions and has been implicated in gliomagenesis, tumor progression, and treatment resistance [33, 59, 60]. The ECM receptor CD44 might coordinate with glial activities in the tumor microenvironment and its expression at the GBM periphery could provide a reliable biomarker for tumor invasiveness [61–63].

We found an increase in Cx43 + cells and Cx43 expression in the host tissue following the infiltration of GBM in human and mouse models, compared to the organotypic control group. Accordingly, an upregulation of Cx43 has been detected at the tumor edge, potentially to promote tumor invasion [14, 64]. Cx43-KO does not induce any compensation of other connexins such as Cx30 [65], implying that the Cx43 response to GBM may constitute a conserved mechanism across the two species [21].

Cx43 expression changes were related to both the tumor cells and the resident tissue. Cx43 is a well-recognized marker for astrocytes. However, it can be expressed by microglia and other cell types throughout the CNS in particular conditions [66]. Accordingly, we found partial overlap between the CD44 and Cx43 immunofluorescent expression in the human peritumoral microenvironment as well as between GFAP and Cx43 in the mouse acute slices and organotypic GBM-brain tissue co-cultures. Cx43 should facilitate the detachment of GBM cells from the tumor core and enhance the movements in the parenchyma [33], while reactive astrocytes are known to overexpress Cx43 following brain injury and inflammation [67, 68].

The increase in the perinuclear Cx43-expressing cells in the adult brain slice system may result from the proliferation of the injected tumor cells, as demonstrated by Ki67 staining. However, the observed changes in Cx43 expression could also reflect increased transcriptional activity or alterations in its subcellular distribution [21, 69]. Indeed, Cx43 expression is dynamic, and its localization can shift between the cytoplasm and the plasma membrane. Consistent with this dynamic regulation, studies in other tumor models have shown that the subcellular localization of Cx43 varies according to the cellular context. For example, nuclear localization of Cx43 has been reported in breast cancer [51], whereas in GBM stem cells, non-junctional Cx43 interacts with the microtubule network to support cell maintenance and tumorigenicity [70]. In our study, fresh brain slices and 2D cultures of murine GBM cells exhibited Cx43 cytoplasmic-to-membrane distribution ratios of approximately 1 and 0, respectively, indicating that Cx43 is distributed almost equally between the cytoplasmic and membrane compartments in brain tissue, whereas GBM cells express low levels of predominantly membrane-associated Cx43. At 3 dpi, coculture of GBM cells with brain slices increased the cytoplasmic component of the spatial ratio, suggesting a redistribution of Cx43 that may reflect enhanced protein synthesis, intracellular trafficking, or turnover. Together, these observations indicate that Cx43 expression and subcellular localization are

dynamically regulated in astrocytic-like cells, including GBM cells, although the functional significance of these changes remains to be determined.

Blockade of Cx43 hemichannels with GAP19 induced a further upregulation of Cx43 protein levels. In addition, primary human GBM cells exhibited marked changes in morphology and polarization following GAP19 treatment. eGFP-labeled GBM cells adopted an elongated morphology with fusiform bidirectional processes and appeared polarized in a common direction, displaying a palisade-like arrangement reminiscent of the migratory phenotype described for their potential ancestors [71]. Accordingly, astrocyte morphology and polarity are known to undergo profound changes during development in response to alterations in extracellular matrix composition, soluble factors, and cytoskeletal dynamics [72, 73]. It is therefore possible that blockade of Cx43 hemichannels disrupts microenvironment-derived signals that contribute to maintaining GBM cell morphology, thereby promoting the formation of oncostream-like cellular arrangements associated with collective cell movement [74]. Accordingly, GL261 cells exhibited a higher number of cells within the scratch region 4 h after GAP19 treatment compared with the corresponding control. However, as the scratch assay quantifies cell occupancy within the wound area, these findings alone do not establish whether the observed effect reflects a migratory behavior or is influenced by other cellular processes, such as changes in proliferation rate or cell–cell interactions [75].

In conclusion, the present study provides insights into GBM biology and microenvironment, enabling the use of human and mouse organotypic brain slice cultures as valuable tools for basic neuroscience and GBM disease modeling [76]. In particular, our findings highlight glial Cx43 as an important mediator of GBM–microenvironment interactions in both human and mouse models, and suggest that targeting Cx43 hemichannels may represent a promising strategy to further elucidate glioblastoma biology. However, organotypic slice cultures are not devoid of limitations. Tissue slicing induces neuronal axotomy and disrupts vascular and astrocytic long-range connections, triggering reactive gliosis and other injury responses [52]. Cut-induced degeneration persists during the culture period, resulting in localized cell death, tissue remodeling, and progressive collapse of the slice [77]. In particular, truncation of the astrocytic syncytium may alter long-range gap-junctional communication and shift the balance between network-mediated and localized signaling mechanisms, including connexin hemichannel activity [78]. These changes may alter the native three-dimensional anatomical organization and thereby modify the microenvironment. Consequently, synaptic connectivity, firing patterns, intercellular signaling pathways, and cellular morphology may differ from those observed in the intact brain. Culture-induced cellular stress responses, including membrane remodeling and blebbing, may further contribute to these alterations, warranting validation in *in vivo* mouse models. Despite these limitations, human slice cultures remain among the closest models to the in vivo human brain, while the mouse slice cultures reduce the number of animal experiments [52]. Mimicking a better in vitro microenvironment of malignant glioma, including the vasculature or ECM soluble factors, may improve the physiological relevance of ex vivo glioma models [79]. Such advances could facilitate patient-specific drug screening, prompting knowledge and further studies.

Declarations

Acknowledgements and Funding. This work was supported by the Italian Society of Anatomy and Histology, Fellowship 2022 (dedicated to Prof. Manzoli) to A.V; Fondazione Bartolo Longo III Millennio to G.C.; the European Innovation Council (EIC)-Pathfinder Programme (THOR; grant number 101099719; to M.P., C.D.L., and A.V.); #NEXTGENERATIONEU (NGEU) and the Ministry of University and Research (MUR), National Recovery and Resilience Plan (NRRP), project MNESYS (PE0000006) to M.P. and G.C., project SmarthyVision (P2022JRBMB) to A.V.; the ANR (AstroXCite) to N.R.

Author Contributions. A.V. performed the experiments, formal analysis, and writing of the original draft; G.M. contributed to experimental part, data collection, formal analysis, and editing of the original draft. C.D.L and J.M., contributed to the experimental part and reviewing of the original draft. An.V., L.R., A.E. contributed to the experimental part and figures preparation. G.C. contributed to conceptualization and reviewing the original draft. G.H. and J.P. provided the human samples and contributed to data collection, conceptualization and reviewing the original draft. A.V., N.R. and M.P. contributed to funding acquisition, supervision, writing, reviewing and editing of the original draft. All the authors approved the manuscript.

Conflicts of Interest. The authors declare no conflicts of interest.

Data Availability. The data that support the findings of this study are available under reasonable request to the corresponding author.

Ethics Approval. Animal experiments were conducted with approval from the Animal Care and Use Committee under the authorization no. 268/2012-B from the Italian Minister of Health.

Patient Consent. This study was approved by the Comité d'Evaluation et d'Ethique de l'INSERM - IRB00003888 (approval n°21-864). Subjects' consent was obtained according to the Declaration of Helsinki.

Clinical trial registration. Not applicable.

Permission to reproduce material from other sources. Not applicable. The graphic abstract was created using Biorender.com

References

1. Farin A, Suzuki SO, Weiker M et al (2006) Transplanted glioma cells migrate and proliferate on host brain vasculature: A dynamic analysis. Glia 53:799–808. https://doi.org/10.1002/glia.20334
2. De Luca C, Virtuoso A, Papa M et al (2022) Regional Development of Glioblastoma: The Anatomical Conundrum of Cancer Biology and Its Surgical Implication. Cells 11:1349. https://doi.org/10.3390/cells11081349

3. Seker-Polat F, Pinarbasi Degirmenci N, Solaroglu I, Bagci-Onder T (2022) Tumor Cell Infiltration into the Brain in Glioblastoma: From Mechanisms to Clinical Perspectives. Cancers (Basel) 14:443. https://doi.org/10.3390/cancers14020443
4. Gupta RK, Niklasson M, Bergström T et al (2024) Tumor-specific migration routes of xenotransplanted human glioblastoma cells in mouse brain. Sci Rep 14:864. https://doi.org/10.1038/s41598-023-51063-7
5. Virtuoso A, De Luca C, Cirillo G et al (2022) Tumor Microenvironment and Immune Escape in the Time Course of Glioblastoma. Mol Neurobiol 59:6857–6873. https://doi.org/10.1007/s12035-022-02996-z
6. Kirschenbaum D, Xie K, Ingelfinger F et al (2024) Time-resolved single-cell transcriptomics defines immune trajectories in glioblastoma. Cell 187:149–165e23. https://doi.org/10.1016/j.cell.2023.11.032
7. Mettang M, Meyer-Pannwitt V, Karpel-Massler G et al (2018) Blocking distinct interactions between Glioblastoma cells and their tissue microenvironment: A novel multi-targeted therapeutic approach. Sci Rep 8:5527. https://doi.org/10.1038/s41598-018-23592-z
8. Sun Y, Wang X, Zhang DY et al (2025) Brain-wide neuronal circuit connectome of human glioblastoma. Nature 641:222–231. https://doi.org/10.1038/s41586-025-08634-7
9. Venkataramani V, Tanev DI, Strahle C et al (2019) Glutamatergic synaptic input to glioma cells drives brain tumour progression. Nature 573:532–538. https://doi.org/10.1038/s41586-019-1564-x
10. Virtuoso A, Giovannoni R, De Luca C et al (2021) The Glioblastoma Microenvironment: Morphology, Metabolism, and Molecular Signature of Glial Dynamics to Discover Metabolic Rewiring Sequence. Int J Mol Sci 22:3301. https://doi.org/10.3390/ijms22073301
11. Resende FFB, Bai X, Del Bel EA et al (2016) Evaluation of TgH(CX3CR1-EGFP) mice implanted with mCherry-GL261 cells as an in vivo model for morphometrical analysis of glioma-microglia interaction. BMC Cancer 16:72. https://doi.org/10.1186/s12885-016-2118-3
12. Henrik Heiland D, Ravi VM, Behringer SP et al (2019) Tumor-associated reactive astrocytes aid the evolution of immunosuppressive environment in glioblastoma. Nat Commun 10:2541. https://doi.org/10.1038/s41467-019-10493-6
13. Lin C-M, Yu C-F, Huang H-Y et al (2019) Distinct Tumor Microenvironment at Tumor Edge as a Result of Astrocyte Activation Is Associated With Therapeutic Resistance for Brain Tumor. Front Oncol 9:307. https://doi.org/10.3389/fonc.2019.00307
14. McCutcheon S, Spray DC (2022) Glioblastoma-Astrocyte Connexin 43 Gap Junctions Promote Tumor Invasion. Mol Cancer Res 20:319–331. https://doi.org/10.1158/1541-7786.MCR-21-0199
15. Spalletti C, Scalera M, Mori E et al (2025) Inhibitory circuit dysfunction as a potential contributor to cortical reorganization in Glioblastoma progression. Neurobiol Dis 213:106997. https://doi.org/10.1016/j.nbd.2025.106997
16. Meyer J, Yu K, Luna-Figueroa E et al (2024) Glioblastoma disrupts cortical network activity at multiple spatial and temporal scales. Nat Commun 15:4503. https://doi.org/10.1038/s41467-024-

48757-5

17. Hausmann D, Hoffmann DC, Venkataramani V et al (2023) Autonomous rhythmic activity in glioma networks drives brain tumour growth. Nature 613:179–186. https://doi.org/10.1038/s41586-022-05520-4
18. Díaz-Fernández B, Henao-Herreno D, Nieto J et al (2025) Differentiation of tumor versus peritumoral cortex in gliomas by intraoperative electrocorticography. Neuro Oncol 27:1758–1771. https://doi.org/10.1093/neuonc/noaf082
19. Brandao M, Simon T, Critchley G, Giamas G (2019) Astrocytes, the rising stars of the glioblastoma microenvironment. Glia 67:779–790. https://doi.org/10.1002/glia.23520
20. Guillebaud F, Barbot M, Barbouche R et al (2020) Blockade of Glial Connexin 43 Hemichannels Reduces Food Intake. Cells 9:2387. https://doi.org/10.3390/cells9112387
21. Kotini M, Barriga EH, Leslie J et al (2018) Gap junction protein Connexin-43 is a direct transcriptional regulator of N-cadherin in vivo. Nat Commun 9:3846. https://doi.org/10.1038/s41467-018-06368-x
22. Delvaeye T, Vandenabeele P, Bultynck G et al (2018) Therapeutic Targeting of Connexin Channels: New Views and Challenges. Trends Mol Med 24:1036–1053. https://doi.org/10.1016/j.molmed.2018.10.005
23. Tamborini M, Ribecco V, Stanzani E et al (2025) Extracellular Vesicles Released by Glioblastoma Cancer Cells Drive Tumor Invasiveness via Connexin-43 Gap Junctions. https://doi.org/10.1093/neuonc/noaf013. Neuro Oncol noaf013
24. Orellana JA, Froger N, Ezan P et al (2011) ATP and glutamate released via astroglial connexin 43 hemichannels mediate neuronal death through activation of pannexin 1 hemichannels. J Neurochem 118:826–840. https://doi.org/10.1111/j.1471-4159.2011.07210.x
25. Pannasch U, Vargová L, Reingruber J et al (2011) Astroglial networks scale synaptic activity and plasticity. Proc Natl Acad Sci U S A 108:8467–8472. https://doi.org/10.1073/pnas.1016650108
26. Medina-Ceja L, Salazar-Sánchez JC, Ortega-Ibarra J, Morales-Villagrán A (2019) Connexins-Based Hemichannels/Channels and Their Relationship with Inflammation, Seizures and Epilepsy. Int J Mol Sci 20:5976. https://doi.org/10.3390/ijms20235976
27. Chever O, Lee C-Y, Rouach N (2014) Astroglial connexin43 hemichannels tune basal excitatory synaptic transmission. J Neurosci 34:11228–11232. https://doi.org/10.1523/JNEUROSCI.0015-14.2014
28. Schumacher S, Tahiri H, Ezan P et al (2024) Inhibiting astrocyte connexin-43 hemichannels blocks radiation-induced vesicular VEGF-A release and blood-brain barrier dysfunction. Glia 72:34–50. https://doi.org/10.1002/glia.24460
29. Guo A, Zhang H, Li H et al (2022) Inhibition of connexin hemichannels alleviates neuroinflammation and hyperexcitability in temporal lobe epilepsy. Proc Natl Acad Sci U S A 119:e2213162119. https://doi.org/10.1073/pnas.2213162119
30. Donati V, Di Pietro C, Persano L et al (2025) Connexin hemichannel blockade by abEC1.1 disrupts glioblastoma progression, suppresses invasiveness, and reduces hyperexcitability in preclinical

models. Cell Commun Signal 23:391. https://doi.org/10.1186/s12964-025-02370-1

31. Murphy SF, Varghese RT, Lamouille S et al (2016) Connexin 43 Inhibition Sensitizes Chemoresistant Glioblastoma Cells to Temozolomide. Cancer Res 76:139–149. https://doi.org/10.1158/0008-5472.CAN-15-1286
32. Uzu M, Sin WC, Shimizu A, Sato H (2018) Conflicting Roles of Connexin43 in Tumor Invasion and Growth in the Central Nervous System. Int J Mol Sci 19:1159. https://doi.org/10.3390/ijms19041159
33. Sin WC, Aftab Q, Bechberger JF et al (2016) Astrocytes promote glioma invasion via the gap junction protein connexin43. Oncogene 35:1504–1516. https://doi.org/10.1038/onc.2015.210
34. Szatmári T, Lumniczky K, Désaknai S et al (2006) Detailed characterization of the mouse glioma 261 tumor model for experimental glioblastoma therapy. Cancer Sci 97:546–553. https://doi.org/10.1111/j.1349-7006.2006.00208.x
35. Ciraku L, Moeller RA, Esquea EM et al (2021) An Ex Vivo Brain Slice Model to Study and Target Breast Cancer Brain Metastatic Tumor Growth. J Vis Exp. https://doi.org/10.3791/62617
36. Virtuoso A, Galanis C, Lenz M et al (2024) Regional Microglial Response in Entorhino-Hippocampal Slice Cultures to Schaffer Collateral Lesion and Metalloproteinases Modulation. Int J Mol Sci 25:2346. https://doi.org/10.3390/ijms25042346
37. Dossi E, Blauwblomme T, Nabbout R et al (2014) Multi-electrode array recordings of human epileptic postoperative cortical tissue. J Vis Exp e51870. https://doi.org/10.3791/51870
38. Maugeri G, D'Amico AG, Amenta A et al (2020) Protective effect of PACAP against ultraviolet B radiation-induced human corneal endothelial cell injury. Neuropeptides 79:101978. https://doi.org/10.1016/j.npep.2019.101978
39. Miceli M, Dell'Aversana C, Russo R et al (2016) Secretome profiling of cytokines and growth factors reveals that neuro-glial differentiation is associated with the down-regulation of Chemokine Ligand 2 (MCP-1/CCL2) in amniotic fluid derived-mesenchymal progenitor cells. Proteomics 16:674–688. https://doi.org/10.1002/pmic.201500223
40. Marques-Torrejon MA, Gangoso E, Pollard SM (2018) Modelling glioblastoma tumour-host cell interactions using adult brain organotypic slice co-culture. Dis Model Mech 11:dmm031435. https://doi.org/10.1242/dmm.031435
41. Gump JM, Dowdy SF (2007) TAT transduction: the molecular mechanism and therapeutic prospects. Trends Mol Med 13:443–448. https://doi.org/10.1016/j.molmed.2007.08.002
42. Lissoni A, Wang N, Nezlobinskii T et al (2020) Gap19, a Cx43 Hemichannel Inhibitor, Acts as a Gating Modifier That Decreases Main State Opening While Increasing Substate Gating. Int J Mol Sci 21:7340. https://doi.org/10.3390/ijms21197340
43. De Bock M, De Smet M, Verwaerde S et al (2022) Targeting gliovascular connexins prevents inflammatory blood-brain barrier leakage and astrogliosis. JCI Insight 7:e135263. https://doi.org/10.1172/jci.insight.135263

44. Dossi E, Zonca L, Pivonkova H et al (2024) Astroglial gap junctions strengthen hippocampal network activity by sustaining afterhyperpolarization via KCNQ channels. Cell Rep 43:114158. https://doi.org/10.1016/j.celrep.2024.114158
45. Cirillo G, Colangelo AM, Bianco MR et al (2012) BB14, a Nerve Growth Factor (NGF)-like peptide shown to be effective in reducing reactive astrogliosis and restoring synaptic homeostasis in a rat model of peripheral nerve injury. Biotechnol Adv 30:223–232. https://doi.org/10.1016/j.biotechadv.2011.05.008
46. Croft CL, Noble W (2018) Preparation of organotypic brain slice cultures for the study of Alzheimer's disease. F1000Res 7:592. https://doi.org/10.12688/f1000research.14500.2
47. Bissen D, Kracht MK, Foss F, Acker-Palmer A (2022) Expansion microscopy of mouse brain organotypic slice cultures to study protein distribution. STAR Protoc 3:101507. https://doi.org/10.1016/j.xpro.2022.101507
48. Pallud J, Varlet P, Devaux B et al (2010) Diffuse low-grade oligodendrogliomas extend beyond MRI-defined abnormalities. Neurology 74:1724–1731. https://doi.org/10.1212/WNL.0b013e3181e04264
49. Trevisi G, Mangiola A (2023) Current Knowledge about the Peritumoral Microenvironment in Glioblastoma. Cancers (Basel) 15:5460. https://doi.org/10.3390/cancers15225460
50. Ylagan LR, Quinn B (1997) CD44 expression in astrocytic tumors. Mod Pathol 10:1239–1246
51. Pilarczyk G, Papenfuß F, Bestvater F, Hausmann M (2019) Spatial Arrangements of Connexin43 in Cancer Related Cells and Re-Arrangements under Treatment Conditions: Investigations on the Nano-Scale by Super-Resolution Localization Light Microscopy. Cancers (Basel) 11:301. https://doi.org/10.3390/cancers11030301
52. Humpel C (2015) Organotypic brain slice cultures: A review. Neuroscience 305:86–98. https://doi.org/10.1016/j.neuroscience.2015.07.086
53. Venkatesh HS, Morishita W, Geraghty AC et al (2019) Electrical and synaptic integration of glioma into neural circuits. Nature 573:539–545. https://doi.org/10.1038/s41586-019-1563-y
54. Bouwen BLJ, Bolleboom A, Tang Y et al (2025) Aberrant neural activity in the peritumoral cortex underlies the progression of tumor-associated seizures. Nat Commun 16:10846. https://doi.org/10.1038/s41467-025-66226-5
55. Harwood DSL, Pedersen V, Bager NS et al (2024) Glioblastoma cells increase expression of notch signaling and synaptic genes within infiltrated brain tissue. Nat Commun 15:7857. https://doi.org/10.1038/s41467-024-52167-y
56. Bak A, Koch H, van Loo KMJ et al (2024) Human organotypic brain slice cultures: a detailed and improved protocol for preparation and long-term maintenance. J Neurosci Methods 404:110055. https://doi.org/10.1016/j.jneumeth.2023.110055
57. Pallud J, Audureau E, Blonski M et al (2014) Epileptic seizures in diffuse low-grade gliomas in adults. Brain 137:449–462. https://doi.org/10.1093/brain/awt345
58. Shojaee P, Weinholtz E, Schaadt NS et al (2025) Biopsy location and tumor-associated macrophages in predicting malignant glioma recurrence using an in-silico model. NPJ Syst Biol Appl 11:3.

https://doi.org/10.1038/s41540-024-00478-7

59. Sin W-C, Crespin S, Mesnil M (2012) Opposing roles of connexin43 in glioma progression. Biochim Biophys Acta 1818:2058–2067. https://doi.org/10.1016/j.bbamem.2011.10.022
60. Wang L, Peng Y, Peng J et al (2018) Tramadol attenuates the sensitivity of glioblastoma to temozolomide through the suppression of Cx43–mediated gap junction intercellular communication. Int J Oncol 52:295–304. https://doi.org/10.3892/ijo.2017.4188
61. Inoue A, Ohnishi T, Nishikawa M et al (2023) Identification of CD44 as a Reliable Biomarker for Glioblastoma Invasion: Based on Magnetic Resonance Imaging and Spectroscopic Analysis of 5-Aminolevulinic Acid Fluorescence. Biomedicines 11:2369. https://doi.org/10.3390/biomedicines11092369
62. Du Z, Wang Y, Liang J et al (2022) Association of glioma CD44 expression with glial dynamics in the tumour microenvironment and patient prognosis. Comput Struct Biotechnol J 20:5203–5217. https://doi.org/10.1016/j.csbj.2022.09.003
63. Lubanska D, Alrashed S, Mason GT et al (2022) Impairing proliferation of glioblastoma multiforme with CD44 + selective conjugated polymer nanoparticles. Sci Rep 12:12078. https://doi.org/10.1038/s41598-022-15244-0
64. Baklaushev VP, Yusubalieva GM, Tsitrin EB et al (2011) Visualization of Connexin 43-positive cells of glioma and the periglioma zone by means of intravenously injected monoclonal antibodies. Drug Deliv 18:331–337. https://doi.org/10.3109/10717544.2010.549527
65. Pridham KJ, Shah F, Hutchings KR et al (2022) Connexin 43 confers chemoresistance through activating PI3K. https://doi.org/10.1038/s41389-022-00378-7. Oncogenesis 11:2
66. Jiang H, Zhang Y, Wang Z-Z, Chen N-H (2023) Connexin 43: An Interface Connecting Neuroinflammation to Depression. Molecules 28:1820. https://doi.org/10.3390/molecules28041820
67. Theodoric N, Bechberger JF, Naus CC, Sin W-C (2012) Role of gap junction protein connexin43 in astrogliosis induced by brain injury. PLoS ONE 7:e47311. https://doi.org/10.1371/journal.pone.0047311
68. Colangelo AM, Cirillo G, Lavitrano ML et al (2012) Targeting reactive astrogliosis by novel biotechnological strategies. Biotechnol Adv 30:261–271. https://doi.org/10.1016/j.biotechadv.2011.06.016
69. Ochalski PA, Sawchuk MA, Hertzberg EL, Nagy JI (1995) Astrocytic gap junction removal, connexin43 redistribution, and epitope masking at excitatory amino acid lesion sites in rat brain. Glia 14:279–294. https://doi.org/10.1002/glia.440140405
70. Smyth JW, Guo S, Chaunsali L et al (2025) Cytoplasmic connexin43-microtubule interactions promote glioblastoma stem-like cell maintenance and tumorigenicity. Cell Death Dis 16:388. https://doi.org/10.1038/s41419-025-07514-2
71. John Lin C-C, Yu K, Hatcher A et al (2017) Identification of diverse astrocyte populations and their malignant analogs. Nat Neurosci 20:396–405. https://doi.org/10.1038/nn.4493

72. Purvis EM, O'Donnell JC, Cullen DK (2022) Unique Astrocyte Cytoskeletal and Nuclear Morphology in a Three-Dimensional Tissue-Engineered Rostral Migratory Stream. Neuroglia 3:41–60. https://doi.org/10.3390/neuroglia3010003
73. Etienne-Manneville S (2008) Polarity proteins in glial cell functions. Curr Opin Neurobiol 18:488–494. https://doi.org/10.1016/j.conb.2008.09.014
74. Kang S, Ughetta ME, Zhang JY et al (2025) Glioblastoma shift from bulk to infiltrative growth is guided by plexin-B2-mediated microglia alignment in invasive niches. Nat Cancer 6:1505–1523. https://doi.org/10.1038/s43018-025-00985-4
75. Molefe PF, Ghasemishahrestani Z, Khumalo NP, Bayat A (2026) The In Vitro Wound-Scratch Assay: Applications, Technical Advances, and Limitations in Wound Healing Research. Int Wound J 23:e70964. https://doi.org/10.1111/iwj.70964
76. Mauro A, Mohamed S (2020) Three dimensional heat and mass transfer in human eye based on porous medium approach. Int J Heat Mass Transf 158:119994. https://doi.org/10.1016/j.ijheatmasstransfer.2020.119994
77. Lossi L, Alasia S, Salio C, Merighi A (2009) Cell death and proliferation in acute slices and organotypic cultures of mammalian CNS. Prog Neurobiol 88:221–245. https://doi.org/10.1016/j.pneurobio.2009.01.002
78. Rouach N, Avignone E, Même W et al (2002) Gap junctions and connexin expression in the normal and pathological central nervous system. Biol Cell 94:457–475. https://doi.org/10.1016/s0248-4900(02)00016-3
79. De Luca C, Papa M (2016) Looking Inside the Matrix: Perineuronal Nets in Plasticity, Maladaptive Plasticity and Neurological Disorders. Neurochem Res 41:1507–1515. https://doi.org/10.1007/s11064-016-1876-2

Figures

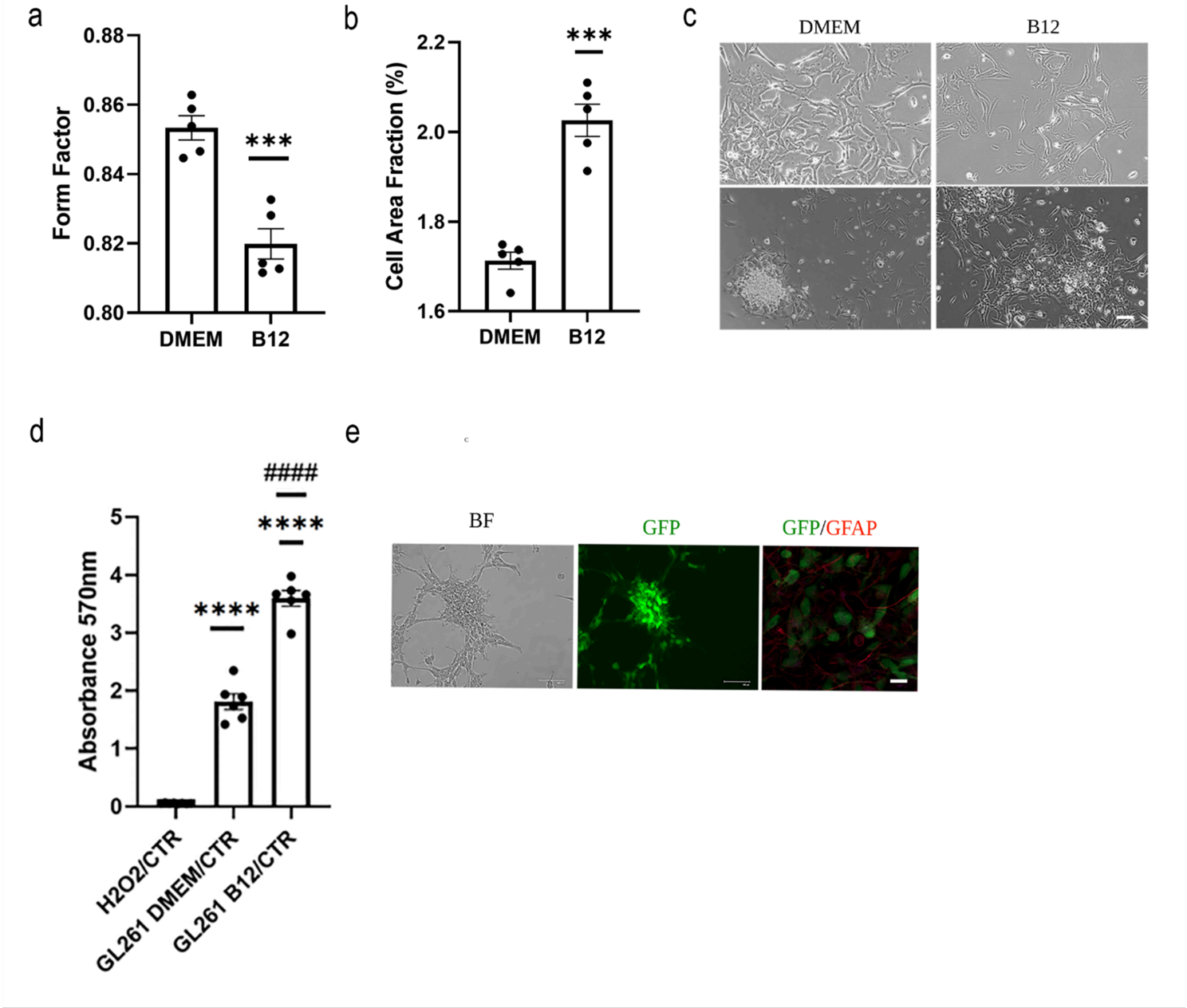


Figure 1

Characterization of GBM cells **(a)** Quantitative analysis of form factor for GL261 cells cultured in DMEM or B12 medium. Data are presented as mean ± SEM. Statistical significance was assessed using an unpaired two-tailed Student's *t*-test with Welch's correction. (A p-value < 0.05 was considered statistically significant; p= 0.0004, t=5.992, df=7.615). Each data point represents an individual biological replicate. **(b)** Quantitative analysis of the cell area fraction (%) covered by GL261 cells cultured in DMEM or B12 medium. Data are presented as mean ± SEM. (p= 0.0002, unpaired two-tailed Student's *t*-test with Welch's correction, t=7.682, df=6.088). Each data point represents an individual biological replicate. **(c)**Morphological features of GL261 cells grown in DMEM/10% FBS (DMEM) and B12-enriched medium (B12). (Up) GL261 in monolayer, (bottom) GL261 forming spheres. Scale bar 50 µm. **(d)** Viability test using MTT substrate for GL261 cells grown in DMEM/10% FBS and B12-enriched medium (One-way

ANOVA, Tukey's multiple comparison test, F (2,17), df=2, p<0.0001. * was used for comparison to the technical control (CTR), # was used for intergroup statistical significance). **(e)** Morphological features of human primary GFP+-N2 cells. BF=bright field; GFP = green fluorescent protein, green; GFAP = Glial fibrillary acidic protein, red. Scale bar 100 µm.

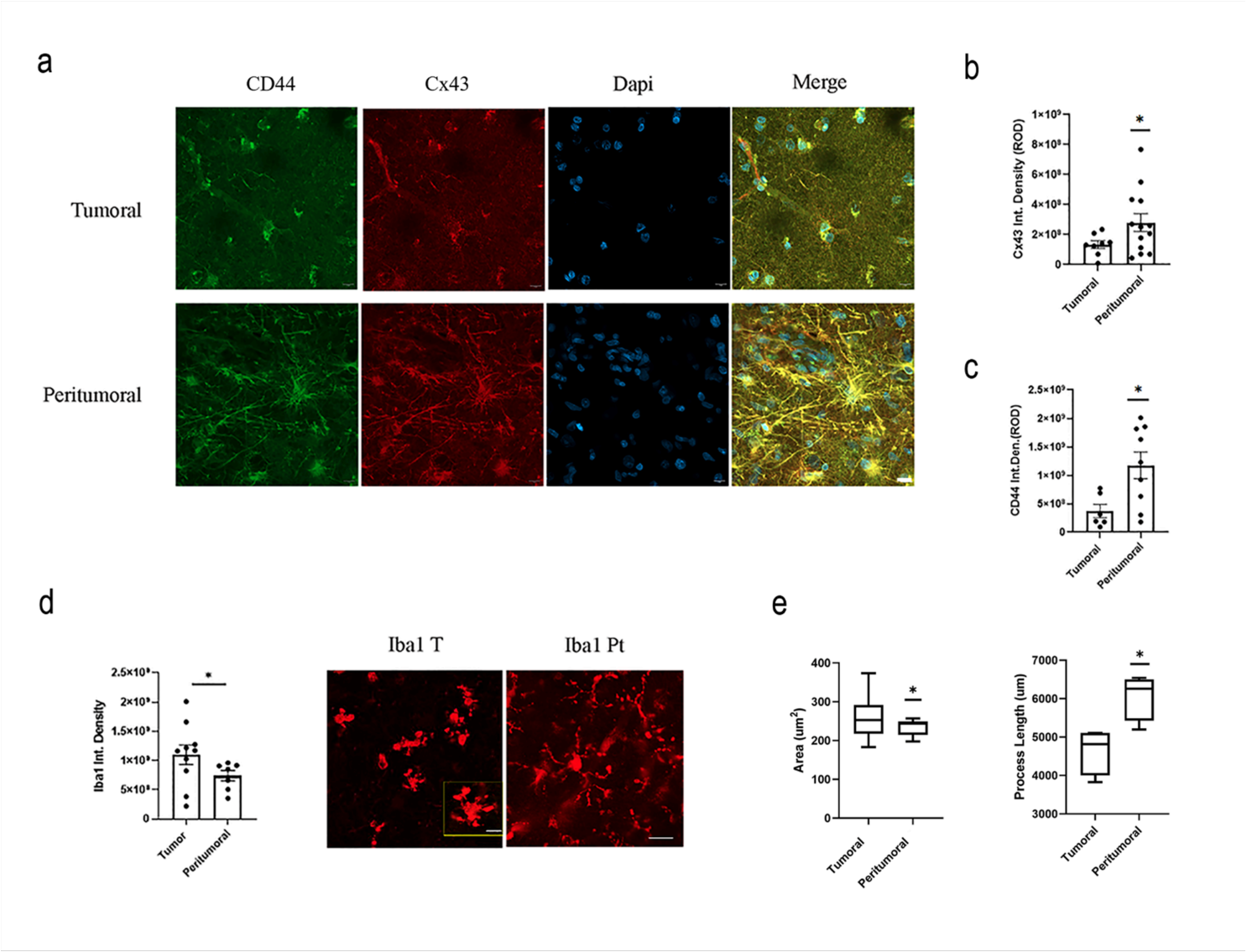


Figure 2

***Characterization of acute human tissue microenvironment from patients with glioma*. (a)** Representative immunofluorescence for CD44 and Cx43 expression in acute brain slices among tumoral and peritumoral tissue. Nuclei were stained by DAPI (blue). Scale bar 20µm. (**b**) Relative quantification of Cx43 intensity from confocal imaging of acute tissue slices among tumoral and peritumoral areas(p=0.0366, two tailed unpaired t-test with Welch's correction, t=2.282, df=15.90). Each data point represents an individual biological replicate. (**c**) Relative quantification of CD44 intensity from confocal imaging of acute tissue slices among tumoral and peritumoral tissue (p= 0.02, two-tailed unpaired t-test, t=2,643, df=13). Each data point represents an individual biological replicate. (**d**) Representative immunofluorescence imaging for Iba1 positive cells in acute tissue slices among tumoral and

peritumoral areas, and relative quantification of signal intensity (p=0.021, Kolmogorov-Smirnov test). Scale bar 50µm; 100 µm for the inset magnification. Each data point represents an individual biological replicate. (**e**) Morphometric measurement of Iba1+ cells from confocal imaging of acute tissue slices among tumoral and peritumoral areas (Mean cell area, F test to compare variances; *p= 0.0250; *n*= 10 tumoral and *n* = 7 peritumoral biological replicates), (processes length, p=0.0058, two tailed unpaired t-test; *n* = 4 tumoral and *n*= 4 peritumoral biological replicates).

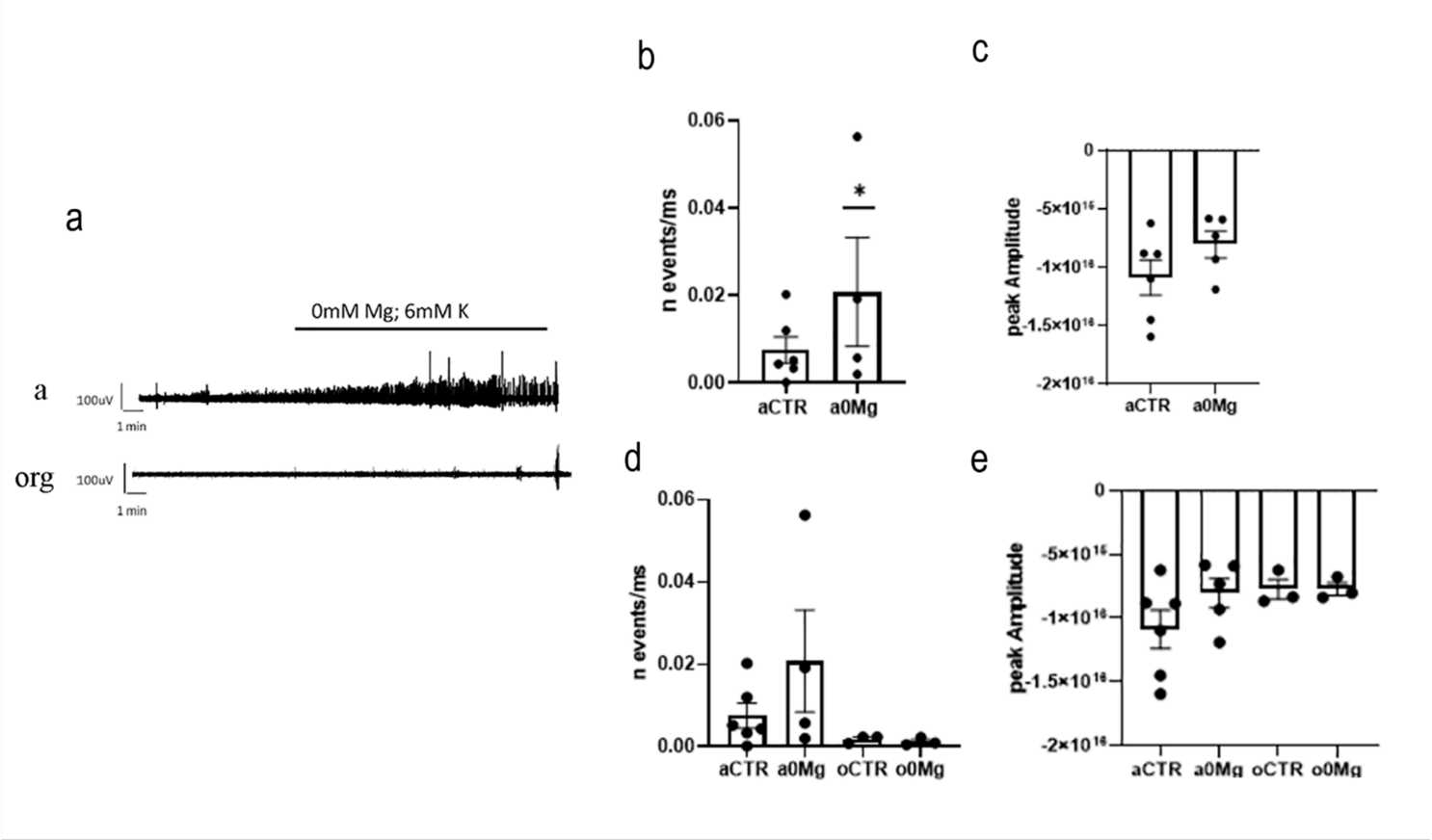


Figure 3

Electrophysiological characterization of acute human tissue from patients with glioma and organotypic conditions. (**a**) Representative multi-electrode array (MEA) recordings in human acute and organotypic brain slices perfused with artificial cerebrospinal fluid (ACSF; left) or ACSF supplemented with 0 mM Mg^{2+} and 6 mM K^{+} (right). Abbreviations: *a*, acute; *org*, organotypic. Each data point represents one biological replicate. (**b**) Spike frequency analysis in human acute brain slices perfused with artificial cerebrospinal fluid (ACSF; left) or ACSF supplemented with 0 mM Mg^{2+} and 6 mM K^{+} (right). (*p = 0.0225, F test for variance, df = 3.3). Abbreviations: *a*, acute; *org*, organotypic. Each data point represents a biological replicate. (**c**) Spike amplitude analysis in human acute brain slices perfused with artificial cerebrospinal fluid (ACSF; left) or ACSF supplemented with 0 mM Mg^{2+} and 6 mM K^{+} (right). Abbreviations: *a*, acute; *org*, organotypic. Each data point represents one biological replicate. (**d**) Comparative analysis of frequency of electrical spikes in acute and organotypic conditions. Each data

point represents a biological replicate. (**e**) Comparative analysis of amplitude of electrical spikes in acute and organotypic conditions. Each data point represents a biological replicate.

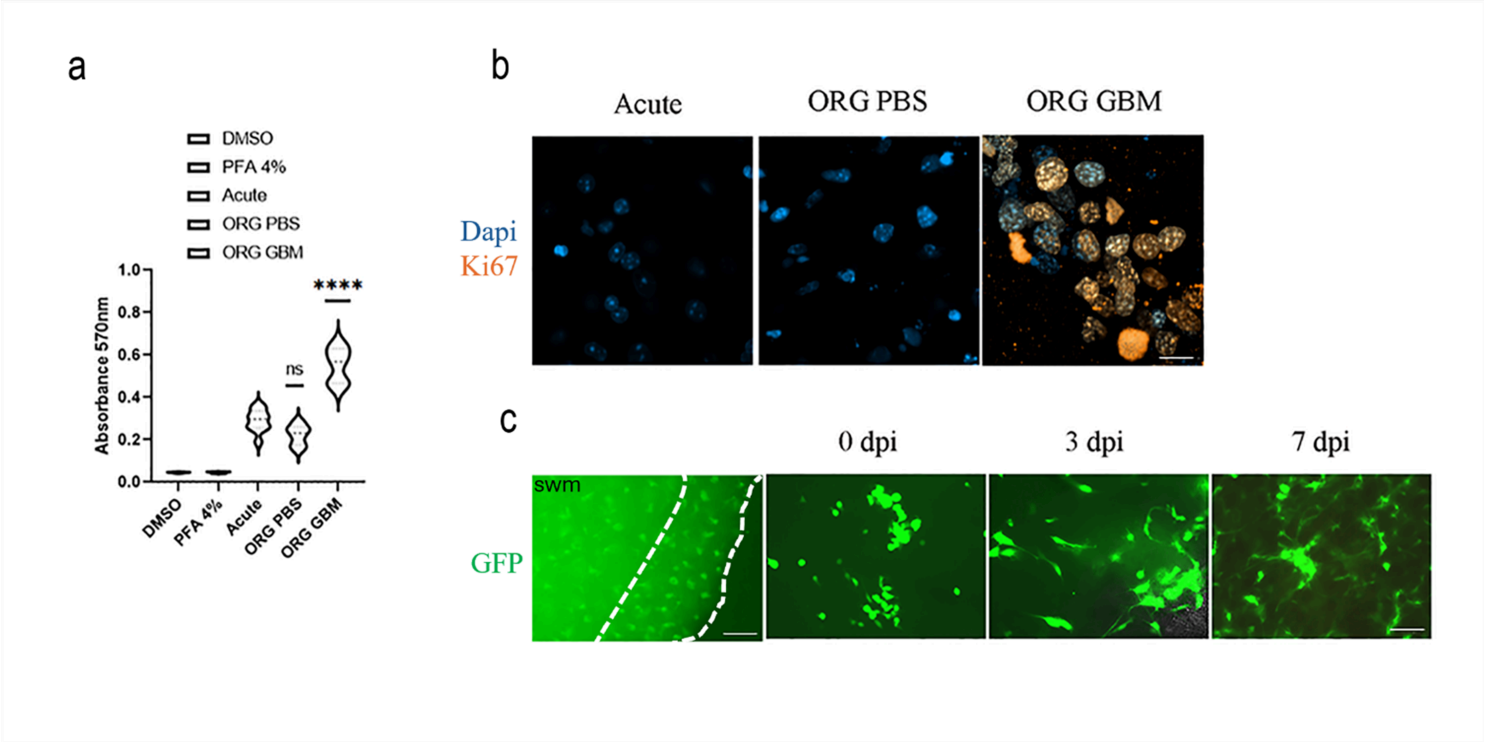


Figure 4

Glioblastoma infiltrates the microenvironment in the organotypic models.

(**a**) MTT viability test of mouse organotypic slice cultures in acute and organotypic condition, with PBS or GBM injection at 3 days post-transplantation (dpi). DMSO=CTR, PFA 4%=Negative CTR ($p \leq 0.0001$, One-way Anova followed by Tukey's test for multiple comparisons, n = 9 (DMSO), n=7 (PFA 4%), n =10 (Acute), n =15 (ORG PBS), and n = 4 (ORG GBM) independent acute slices/ slices cultures). (**b**) Representative panel for immunofluorescence of the proliferative marker ki67 (orange) in the gray matter of murine acute and organotypic slices cultures, with PBS or GL261 cells injection. Nuclei are stained by DAPI (blue). Scale bar 20µm. (**c**) Representative dynamic microscopy images of transplanted eGFP-labeled GBM cells of human cortical tissue at 0, 3, and 7 dpi. Scale bar: 100 µm. High-magnification images were acquired from the gray matter of the peritumoral region of the organotypic tissue, included between the dashed lines. The low-magnification dark-field image at 3 dpi (left) was overlaid with the corresponding bright-field image to visualize the tissue background. Scale bar: 100 µm; swm = subcortical white matter.

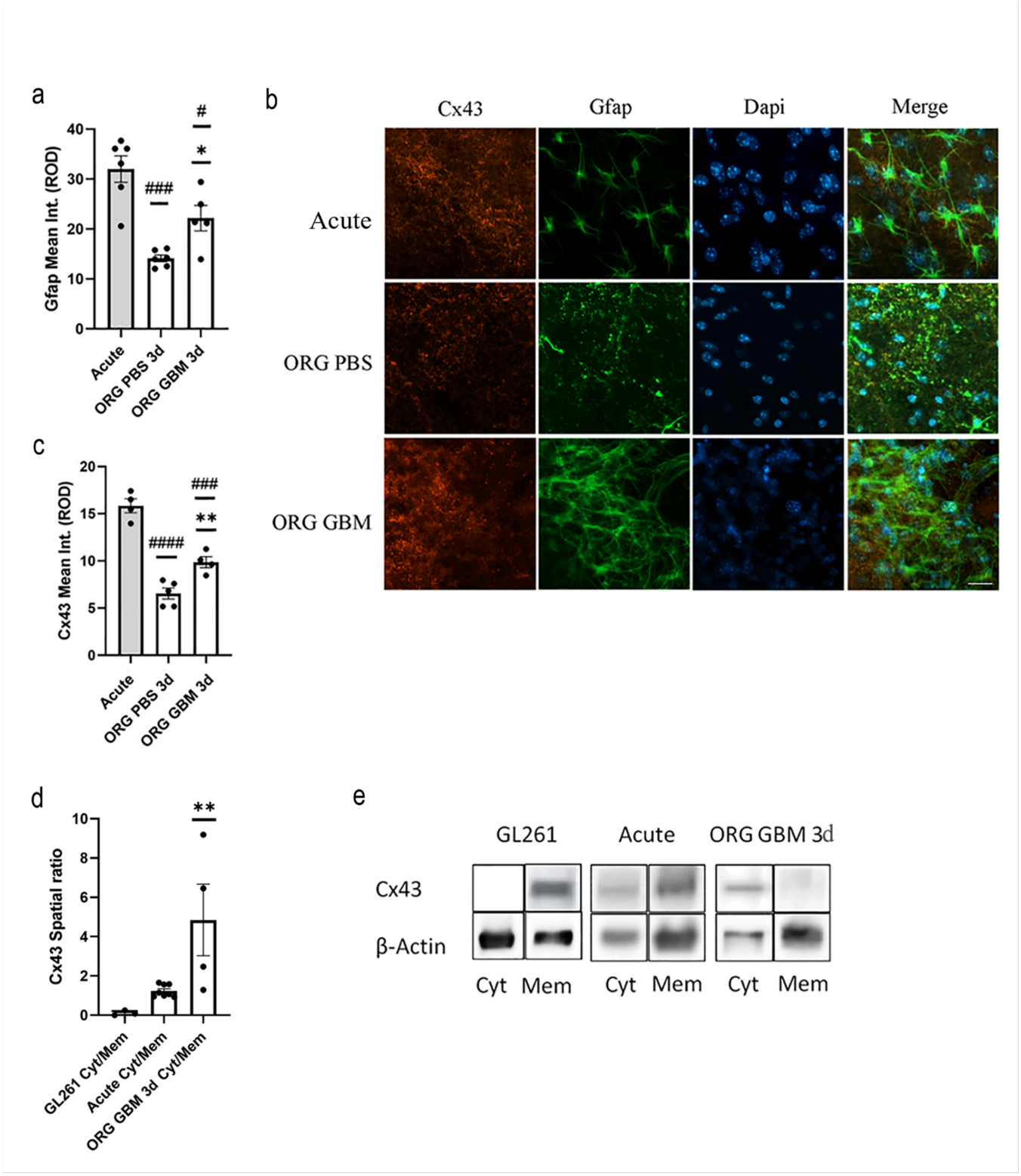


Figure 5

Glioblastoma infiltration modifies the mouse microenvironment.

(a) Analysis of GFAP fluorescence intensity in acute and organotypic slices following PBS or GBM injection. *p ≤ 0.05 versus the organotypic (ORG) PBS group; #p ≤ 0.05 versus the corresponding acute group (One-way Anova followed by Tukey's test for multiple comparisons, Acute vs Org PBS, $^{\#}$p=0.0001;

Acute vs Org GBM, #p= 0.015; Org PBS vs Org GBM, *p=0.0468). Each data point represents an individual biological replicate. **(b)** Representative immunofluorescence images for GFAP and Cx43 acquired by using confocal microscopy of acute and organotypic tissue slices, following PBS or GBM injection. Nuclei were stained with DAPI (blue). Scale bar: 20 μm. **(c)** Analysis of Cx43 fluorescent signal intensity in acute and organotypic slices, following PBS or GBM injection. (*p ≤ 0.05 versus the organotypic (ORG) PBS group; #p ≤ 0.05 versus the corresponding acute group, one way Anova followed by Tukey's test, Acute vs ORG PBS, #p=0.0001; Acute vs. ORG GBM #p=0.0002; ORG PBS vs ORG GBM, *p=0.0098). Each data point represents an individual biological replicate. **(d)** Analysis of Cx43 protein localization ratio between the soluble (cytoplasmic) and insoluble (membrane) part from western blotting samples of mouse acute slices, 2D cultures of GL261 cells, and organotypic co-cultures (One-way Anova followed by Kruskal-Wallis test, Org GBM vs Gl261, p= 0.0049; Org GBM vs Acute, p=0.1570). Each data point represents an individual biological replicate. **(e)** Representative western blotting bands from acute slices, 2D cultures of GL261 cells, and organotypic co-cultures from soluble (cyt, cytoplasmic) and insoluble (mem, membrane) parts of the tissues.

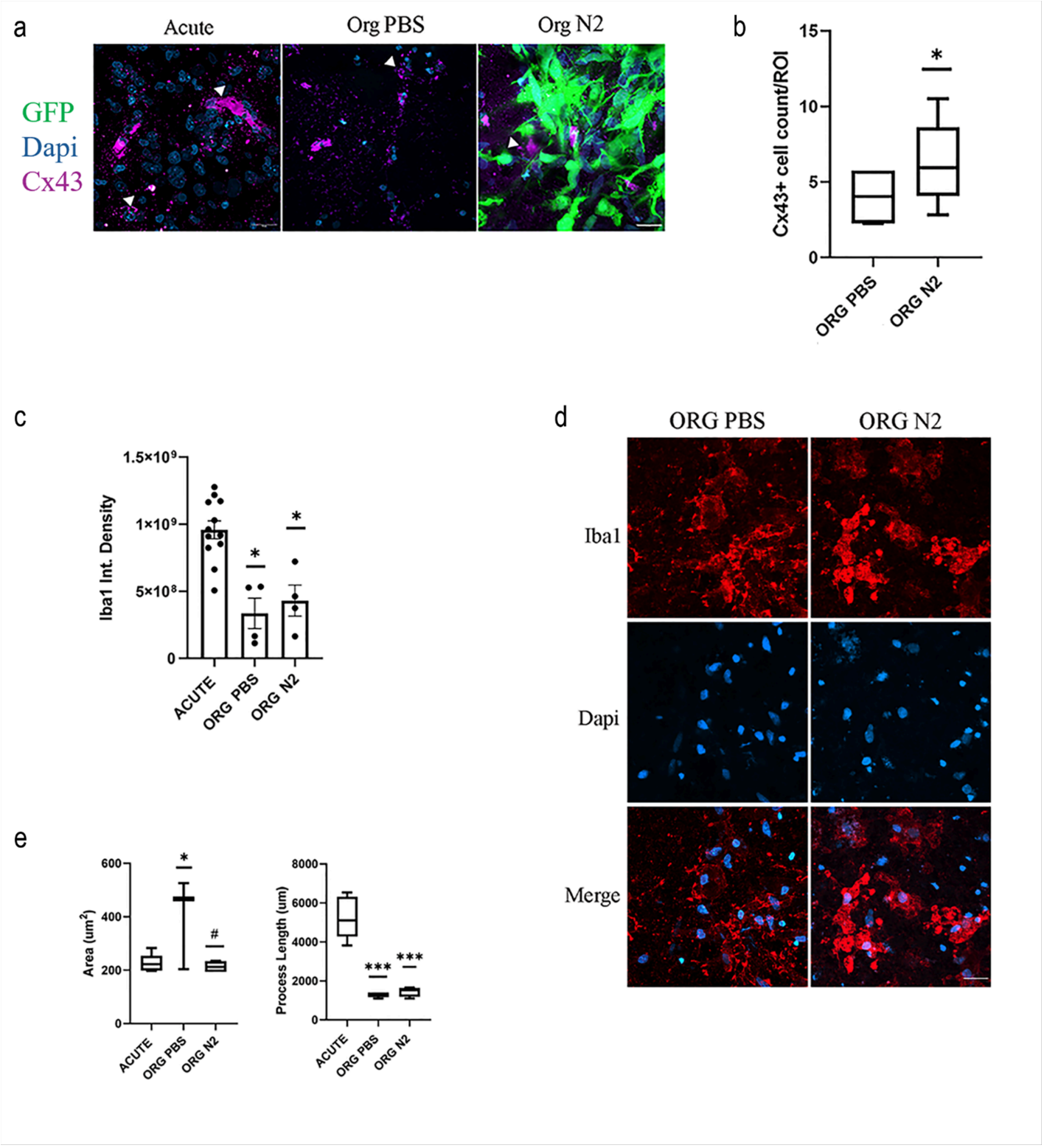


Figure 6

Glioblastoma might change the human microenvironment.

(a) Representative immunofluorescence imaging for human Cx43-positive cells (white arrows) from confocal imaging of human organotypic tissue slices in the CTR group or injected with PBS and/or N2 GFP+ cells. GFP, green; Cx43, purple; DAPI staining for nuclei, blue. Scale bar 20 μm. (**b**) Relative

quantification of perinuclear Cx43-expressing cells per region of interest (ROI) in organotypic tissue slices injected with PBS or N2 GFP+ cells (p= 0.0437, t-test, df=10); ORG PBS *n*=4, ORG N2 *n*=6). (**c-d**) Relative quantification of Iba1 density in acute and organotypic human tissue slices injected with PBS or N2 GFP+ cells (one-way Anova, Dunnet's multiple comparisons test, ACUTE vs ORG PBS, *p= 0.0264; ACUTE vs ORG N2, *p= 0.0415), and representative confocal imaging. Iba1, red. Nuclei were stained using DAPI (blue). Scale bar, 20 µm. Each data point represents an individual biological replicate. (**e**) Morphometric measurements of area and process length for Iba1+ cells from confocal imaging of acute and organotypic tissues injected with PBS or N2 GFP+ cells. Ordinary One-way Anova followed by Tukey's multiple comparisons test (regarding area, ACUTE vs ORG PBS, *p=0.0334; ORG PBS vs ORG N2, #p=0.0323; regarding processes length, ACUTE vs ORG PBS, *p≤0.0001; ACUTE vs ORG GBM, *p≤0.0001; Acute, *n*= 8; ORG PBS *n*=4; ORG N2 *n*=4).

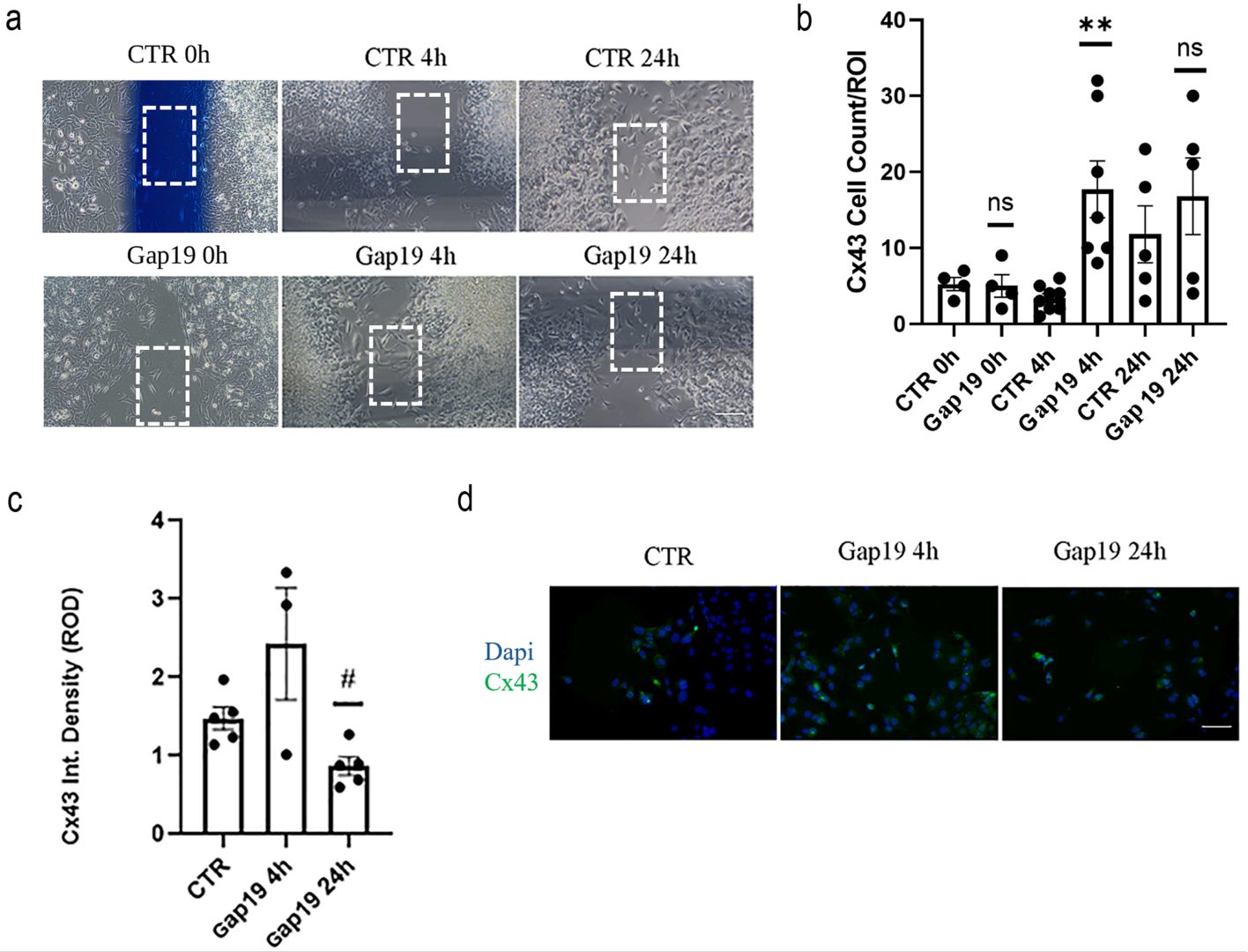


Figure 7

Effect of GAP19 on GL261 cell migration and Cx43 expression.

(a-b) Scratch assay quantification of the migratory ability of GL261 cells under control (CTR) conditions or following treatment with GAP19 (200 µM) at 0, 4, and 24 h, and representative images. The scratch area is labelled in blue in the first image (top left). The region of interest (ROI) used for quantification is outlined by a dashed line. Scale bar: 50 µm. Data points represent independent biological replicate (p=0.004, Ordinary One way Anova followed by Tukey's multiple comparisons test, *,p≤0.05 **p≤0.01). **(c-d)** Representative immunofluorescence images showing Cx43 expression in GL261 cells under control (CTR) conditions or after treatment with GAP19 (200 µM) for 4 and 24 h, and the corresponding quantitative analysis ($^{\#}$p= 0.014, one-way Anova, Tukey's multiple comparisons test). Data points represent independent biological replicates. Cx43 is shown in green and nuclei are counterstained with DAPI (blue). Scale bar: 50 µm.

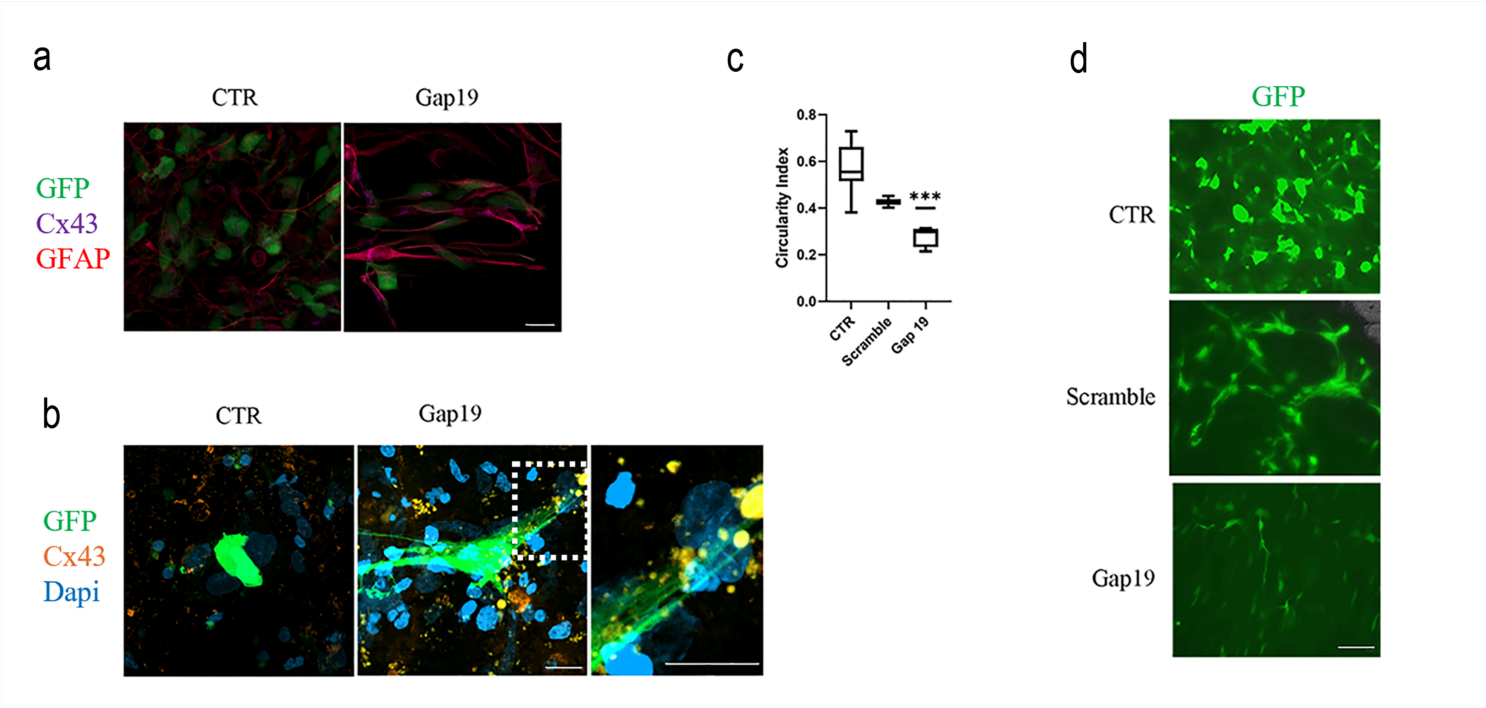


Figure 8

Cx43 protein expression in human models and the GAP19 effect

(**a**) Representative imaging for GFP+ N2 cells in CTR conditions or under treatment with GAP19 200 µM. (GFP, green; GFAP, magenta; Cx43, violet). Scale bar 20 µm. (**b**) Representative immunofluorescence for Cx43 (orange) of GFP+ N2 cells in co-culture with human peritumoral organotypic slices, in CTR conditions or under treatment with GAP19 200 µM, and detail included in the dashed line frame. Nuclei were stained with DAPI. Scale bar: 20 µm and 16 um, respectively. **(c)** Representative imaging for GFP+ N2 cells in co-culture with human peritumoral organotypic slices, in CTR conditions or under treatment with scramble peptide or GAP19 200 µM. (GFP, green). **(d)** N2 GFP+cells morphometry in co-culture with human peritumoral organotypic slices, in CTR conditions or under treatment with GAP19 200 µM (Ordinary one-way ANOVA, Tukey's multiple comparisons test, *p=0.0006; CTR *n*=9, Scramble *n*= 3, Gap-19 *n*= 4. Data points represent independent biological replicates.

Supplementary Files

This is a list of supplementary files associated with this preprint. Click to download.

- Table1.tif
- SupplementaryFigures.doc